ELSEVIER

Fine Spatial Resolution Simulated Satellite Sensor Imagery for Land Cover Mapping in the United Kingdom

Paul Aplin, Peter M. Atkinson,* and Paul J. Curran**

This article presents a set of techniques developed to classify land cover on a per-parcel (herein termed per-field) basis by integrating fine spatial resolution simulated satellite sensor imagery with digital vector data. Classification, based on the spectral and spatial properties of the imagery, was carried out on a per-pixel basis. The resulting classified images were then integrated with vector data to classify on a per-field basis. Four tools were adopted or developed to increase the accuracy and utility of the per-field classification and a fifth was proposed. The spectral variability within agricultural fields resulted in misclassification within the per-pixel classification, and this was overcome using a per-field classification. Mixed land cover in urban areas also resulted in misclassification. A low pass smoothing filter and a "texture" filter applied to the per-pixel classified image increased the classification accuracy of this land cover prior to per-field classification. The flexibility of the integration process enabled the exploitation of spectral and spatial variation between pixels within individual parcels to produce new classes during per-field classification and to identify fields with a high likelihood of misclassification.

INTRODUCTION

Land cover mapping at local to national scales has been hindered by the relatively coarse spatial resolution of satellite sensor imagery (Townshend, 1992; Johnsson, 1994; Harris and Ventura, 1995). For example, the Land Cover Map (LCM) of Great Britain, was generated using Landsat Thematic Mapper (TM) imagery with a spatial resolution of 30 m and a routinely mapped parcel size of no less than 1 ha (Fuller et al., 1994). Satellite sensor imagery with a spatial resolution of 1 m in panchromatic mode and 4 m in multispectral mode will become widely available over the next few years, as a result of a post-Cold War relaxation of governmental legislation on remote sensing from space (Aplin et al., 1997a). These new sources of fine spatial resolution imagery will increase the amount of information attainable on land cover at local to national scales (Aplin and Atkinson, 1997). In particular, the minimum parcel size at which mapping takes place will be considerably smaller than that of contemporary surveys, and this will result in an increase in geometric detail and accuracy.

Associated with an increase in spatial resolution is, commonly, an increase in the internal variability within remotely sensed land cover parcels, which can lead to a decrease in classification accuracy at the per-pixel level (Townshend, 1981; 1992; Cushnie, 1987). This problem can be alleviated by per-parcel (herein termed per-field) classification techniques, which involve analyzing groups of pixels within land cover parcels. Per-field classification, through an analysis of data at the scale of the mapping unit (such as the agricultural field or area of a given housing type), may lead to an increase in classification accuracy over that of a per-pixel classification (Mason et al., 1988; Pedley and Curran, 1991; Johnsson, 1994; Harris and Ventura, 1995; Janssen and Molenaar, 1995) and the results may be easier to interpret (Ryherd and Woodcock, 1996).

Per-field classification, through the integration of remotely sensed imagery and digital vector data, has been used to generate, albeit crudely, land cover information for more than a decade (Catlow et al., 1984). Develop-

* Department of Geography, University of Southampton, Highfield, Southampton, United Kingdom

Address correspondence to Paul Aplin, Dept. of Geography, Univ. of Southampton, Highfield, Southampton SO17 1BJ, UK. E-mail: aplin@soton.ac.uk

Received 15 July 1998; revised 24 November 1998.

REMOTE SENS. ENVIRON. 68:206–216 (1999)

655 Avenue of the Americas, New York, NY 10010

0034-4257/99/$–see front matter
PII S0034-4257(98)00112-6

Table 1. Characteristics of Image Acquisition

Date of acquisition	1 May 1996
Time of acquisition	Between 11:45 h and 12:15 h
Number of flightlines	Four
Direction of flightlines	South–north
Sensor mode	Spatial
Spatial resolution	4 m
Spectral wavebands	450–520 nm, 520–600 nm, 630–690 nm, 760–900 nm
Data format	16 bit
Altitude	1280 m
View angle	Nadir
Field of view	78°
Swath width	1.9 km
Solar elevation angle	60.08°
Solar azimuth angle	180.74°
Status of atmosphere	Patchy cloud cover at 1520 m

ments in technology mean that sophisticated integration is now possible (Cowen et al., 1995) and per-field classification is now available within several geographical information systems (GIS) such as ARC/INFO (ESRI, 1993).

Following an early per-field classification using Landsat MSS imagery with a spatial resolution of 57 m by 79 m (Catlow et al., 1984) subsequent researchers have applied per-field classification techniques to imagery with ever finer spatial resolutions. Janssen et al. (1990), Harris and Ventura (1995), Janssen and Molenaar (1995), and Lobo et al. (1996) performed per-field classifications on Landsat TM imagery with a spatial resolution of 30 m, and Pedley and Curran (1991), Johnsson (1994), and Mégier et al. (1984) performed per-field classifications on Satellite Pour l'Observation de la Terre (SPOT) High Resolution Visible (HRV) and simulated SPOT HRV imagery with a spatial resolution of 20 m. The success of per-field classification depends on many factors, notably the relationship between the spectral and spatial properties of the imagery, the size and shape of the fields, and the land cover classes used (Janssen and Molenaar, 1995). However, per-field classification accuracies were consistently higher than those of per-pixel classification in the studies mentioned above.

Despite the demonstrated success of per-field classification, technological limitations remain. There have been several calls for the use of raster and vector data together in a GIS (Cowen et al., 1995; White et al., 1995; Congalton, 1997; Ortiz et al., 1997), enabling the development of more accurate and efficient per-field classification techniques. Commonly, however, current approaches to per-field classification involve rasterizing vector data prior to integration with remotely sensed imagery. While this process is easy to implement in a GIS (ESRI, 1993), it can result in a loss of geometric precision (Davis et al., 1991; Ehlers et al., 1991; Hinton, 1996; Wilkinson, 1996; Congalton, 1997).

In this article we discuss a fairly simple and efficient method of per-field classification applied to simulated satellite sensor imagery (with a spatial resolution of 4 m) and rasterized vector data at the local scale. Land cover information was generated with the broader aim of developing techniques using the fine spatial resolution satellite sensor imagery (which will be routinely available later in the decade) for national (UK) scale mapping. We developed and tested four specific tools in order to increase the accuracy and utility of per-field classification (low pass smoothing filter, "texture" filter, production of new classes, error flag) and a fifth tool was proposed (missing boundary flag).

FIELD SITE AND SAMPLE DATA

To carry out the per-field classification, a field site was selected and sample data acquired.

Field Site

A field site on the western fringe of St. Albans, Hertfordshire, United Kingdom was selected that contained a variety of rural and urban land cover types. The rural areas, in the northwest and southwest, were predominantly agricultural with several crops under cultivation and some pasture intermixed with areas of woodland. The urban areas comprised a mixture of industrial, residential and recreational (for example, public parks with a boating lake, school playing fields) land cover.

Data

Three sources of data were used: Compact Airborne Spectrographic Imager (CASI) imagery (Table 1), "LandLine" digital vector data, and ground reference data.

CASI imagery was acquired on 1 May 1996 since most of the land cover classes of interest were distinguishable at this time of year. Particularly, different crop types could be distinguished at this stage of the growing season. Four flightlines of imagery, running south–north, were acquired between 11:45 h and 12:15 h. The field site was thus well illuminated, with a solar elevation of 60.08°. The CASI was operated in spatial mode at an altitude of 1280 m, acquiring imagery with a spatial resolution of 4 m and in four spectral wavebands, to match the specifications of three fine spatial resolution satellite sensors developed by U.S. organizations: QuickBird (by EarthWatch), IKONOS-1 (by Space Imaging), and OrbView-3 (by ORBIMAGE) (Aplin et al., 1997a). With a field of view of 78°, the CASI acquired each image flightline at a swath width of approximately 1.9 km. When combined, the four image flightlines provided complete coverage over an area of 8 km by 5 km on the western edge of St. Albans. Patchy cloud cover at an altitude of 1520 m during image acquisition resulted in areas of cloud shadow covering significant portions of the imagery. Therefore, a cloud shadow-free subset (3 km by 1.5 km), extracted from one of the image flightlines, was

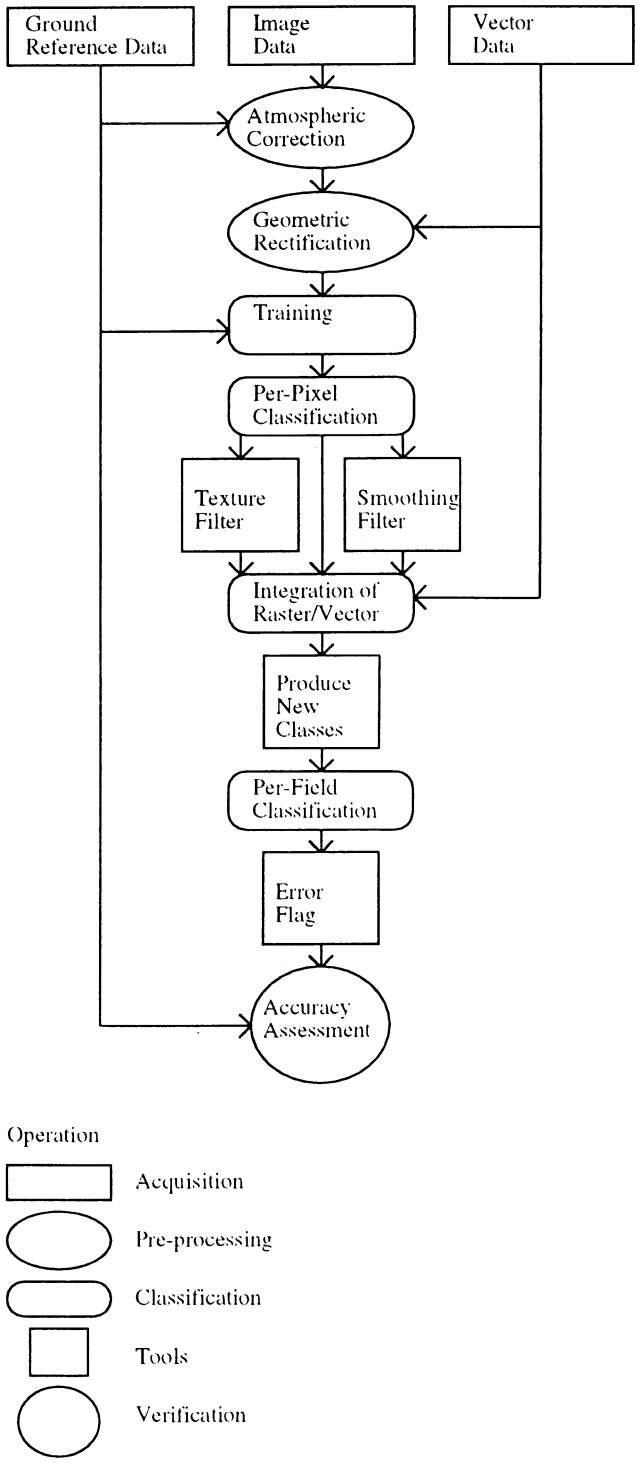

Figure 1. Analytical procedure for per-field classification.

used for further analysis. For full discussions of the technical specifications and radiometric calibration of the CASI see Curran (1994) and Babey and Soffer (1992), respectively.

Land-Line digital vector data were supplied for the 8 km by 5 km study area by the Ordnance Survey. These data comprised points and lines and were registered to the British National Grid (BNG) map coordinate system. Each entity (point and line) had a feature code by which it could be categorized. A vector coverage of the 3 km by 1.5 km field site was created to match exactly the area covered by the image subset.

Ground reference data were acquired from three sources: a radiometric survey, communication with residents, and a land cover survey. The radiometric survey was carried out to collect nadir measurements of radiance that were to be used in the subsequent atmospheric correction of the CASI imagery. Radiometric measurements were taken, concurrently with the CASI image acquisition, of six bright and dark surfaces (winter wheat, winter barley, oilseed rape, grass, water, and tarmac) using a SPECTRON-SE590™ spectroradiometer.

Communication with residents and a land cover survey were carried out to generate a reference land cover map to be used subsequently for training and validating the classified images. Thirty-three residents and land owners at the field site were contacted by post and asked to provide land cover information on proforma maps. Two thirds of these replied. A land cover survey was carried out in the days following image acquisition by a team of ten fieldworkers who mapped land cover in each land cover parcel within the 8 km by 5 km study area. The postal and ground land cover data were combined to generate a reference land cover map of the field site. The reference land cover map recorded the land cover of the field site on a per-field basis. That is, a single land cover class was entered for each field on the reference land cover map.

ANALYSIS

An analytical procedure was developed to classify the CASI imagery using both per-pixel and per-field techniques (Fig. 1).

Preliminary Processing

The fine spatial resolution of the CASI imagery enabled differentiation between similar crop types (such as wheat and barley), seasonal crops (such as winter and spring barley), and woodland categories (such as broadleaved and conifer woodland). Eight classes were selected: wheat, winter barley, spring barley, bare soil (recently ploughed land), grassland, broadleaved woodland, water, and urban.

The CASI image subset was atmospherically corrected by first regressing ground-based radiometric measurements of the six surfaces with spectral values obtained from the imagery and, second, applying these equations to the CASI image. One regression equation was applied per waveband. The image subset was extracted from the center of the swath of the image flightline. Therefore, any differences in atmospheric interference arising from varying path lengths between the

CASI and the center and the edges of the image swath were negligible. Further, since the spectral wavebands were broad (Table 1), they were relatively insensitive to atmospheric interference.

To enable integration of the CASI imagery with the Land-Line data, it was necessary to register the two data sets to a single map coordinate system. Since the Land-Line data were already registered to the BNG, it was decided to register the CASI imagery to the Land-Line data using a mathematical transformation and a nearest neighbor resampling technique.

Per-Pixel Classification

The per-pixel classifier was trained on a representative sample of each of the eight land cover classes on the CASI image prior to per-pixel classification using a maximum likelihood classifier. Training samples were selected using the reference land cover map. Block training was performed, whereby blocks of pixels were selected from the centers of fields of known land cover. This was preferable to point training (the selection of individual pixels for training) since the unit of study was the field. Block training accounted for a degree of within-field variation. Fields of mixed land cover and the edges of fields were not selected for training since these would create a mixed training class.

The classification of the urban area as a single urban land cover class was problematic as it was composed of many distinct land cover types: tarmac, concrete, tiles, grass, and trees (Aplin and Atkinson, 1997). Therefore, a low pass smoothing filter was adopted and a "texture" filter developed for postclassification enhancement. The smoothing filter used the modal value to remove some of the minor land cover components. A drawback of this technique is that filtering is also applied to non-urban areas. While the smoothing of misclassified pixels is desirable, it is possible that small rural fields will be erased. Consequently, a relatively small window of 9 by 9 pixels was used to enable smoothing in urban areas without greatly affecting small rural fields. The "texture" filter removed minor land cover components within the urban area using a 15 by 15 pixel moving window in which the class assigned to the central pixel was a function of the frequency of occurrence of several classes in the window. Specifically, where the window contained a relatively high proportion of "urban" pixels and the remainder of the window was any combination of "non-urban"pixels an urban class was assigned to the central pixel. Where the window contained a relatively low proportion of "urban" pixels the central pixel was unchanged. This technique had two main benefits over smoothing. First, the texture filter was effected only in urban areas so rural areas remained largely unchanged. Second, new urban classes (low-density and high-density urban land cover) were generated based on the texture within the image. That is, where the proportion of "urban" pixels within the window was greater than 50% and less than 100%, the low-density urban class was assigned to the central pixel. Where the proportion of "urban" pixels was 100%, the high density urban class was assigned to the central pixel. Alternatively, where the proportion of "urban" pixels was less than 50%, the central pixel was unchanged.

Per-Field Classification

The three per-pixel classified images [the original classification (Fig. 2a), the smoothed classification (Fig. 3a), and the "texture" filtered classification (Fig. 4a)] were integrated with polygonized Land-Line data to perform three per-field classifications.

Integration was achieved in a GIS by rasterizing the Land-Line data and combining the two raster data sets (CASI, Land-Line) in a single raster grid. When rasterized, each Land-Line polygon was represented by a pixel or a contiguous group of pixels that most closely matched its spatial properties. The precise location of each polygon (as determined by its point coordinates) was, therefore, lost as Land-Line data were generalized to a regular raster grid. That is, geometric accuracy decreased. In the rasterizing process, however, the degree to which geometric accuracy is reduced depends on the pixel size of the rasterized data. Generally, the smaller the pixel size, the smaller the decrease in geometric accuracy, although this may also increase data volume and processing time. The Land-Line data were rasterized to a pixel size of 4 m since at this scale there was only a slight loss of geometric accuracy. Further, this pixel size matched the spatial resolution of the CASI imagery and enabled a close relationship between the two data sets. The grid of rasterized Land-Line polygons was matched spatially with the classified CASI image such that there was correspondence between the pixels of each. Per-field classification was then performed by calculating the modal land cover class (the dominant land cover class) within each field (Land-Line polygon) and applying this class to the entire field. That is, for each Land-Line polygon, the proportion of the polygon covered by each land cover class was calculated. The class with the largest number of pixels (the modal land cover class) was extracted and reassigned to the original vector (non-rasterized) Land-Line polygon. Figures 2b, 3b, and 4b illustrate the per-field original classified image, the per-field smoothed classified image, and the per-field "texture" filtered classified image respectively.

The flexibility of the raster-vector integration process enabled the exploitation of within-field spectral and spatial variation and two further tools were developed to increase the utility of the overall classification process. First, new useful classes were produced at the per-field stage. A fairly simple technique was implemented which used the proportions of land cover classes within each vector polygon rather than the modal class to assign land cover per field. For example, in an earlier study, where

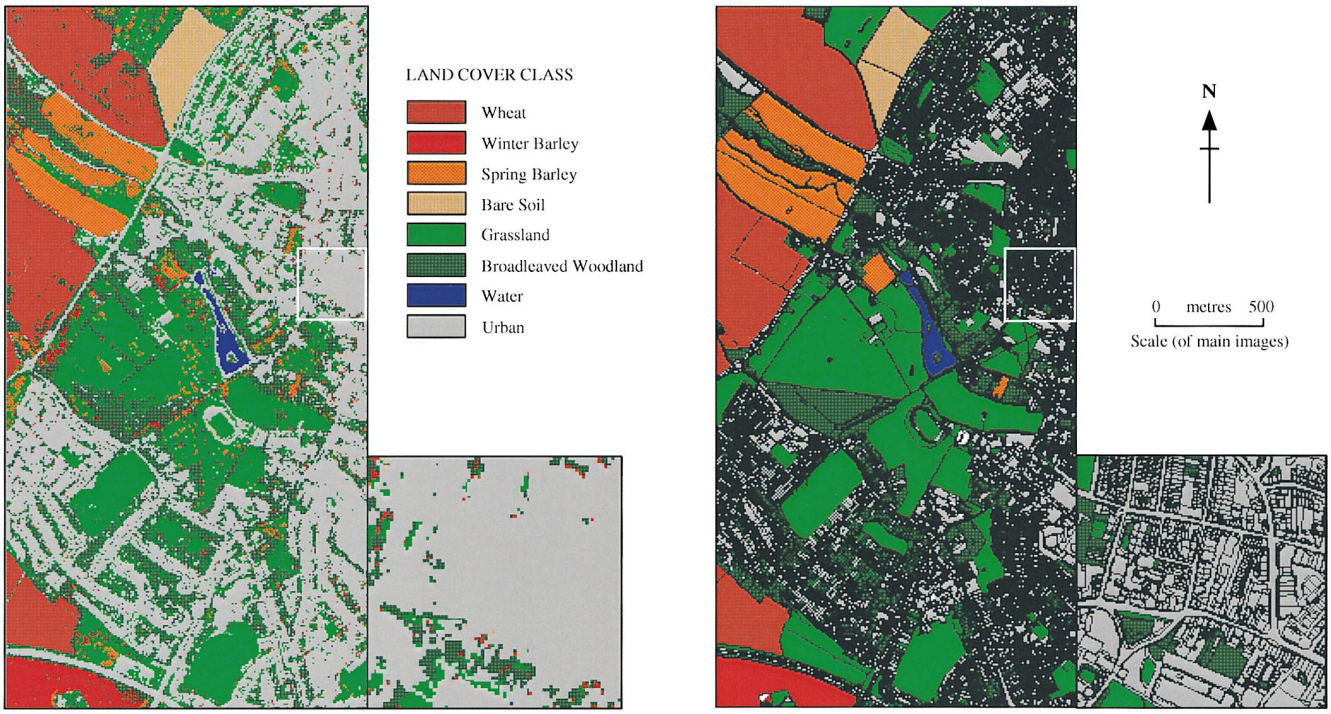

Figure 2. a) Per-pixel and b) per-field original classification of the study area. The black features in the per-field classification are vector boundaries. To the bottom right of each of the main images is an enlargement of the urban area marked by the white box. (© Crown copyright. MC 1275. Used with permission.)

Figure 3. a) Per-pixel and b) per-field smoothed classification of the study area. The black features in the per-field classification are vector boundaries. To the bottom right of each of the main images is an enlargement of the urban area marked by the white box. (© Crown copyright. MC 1275. Used with permission.)

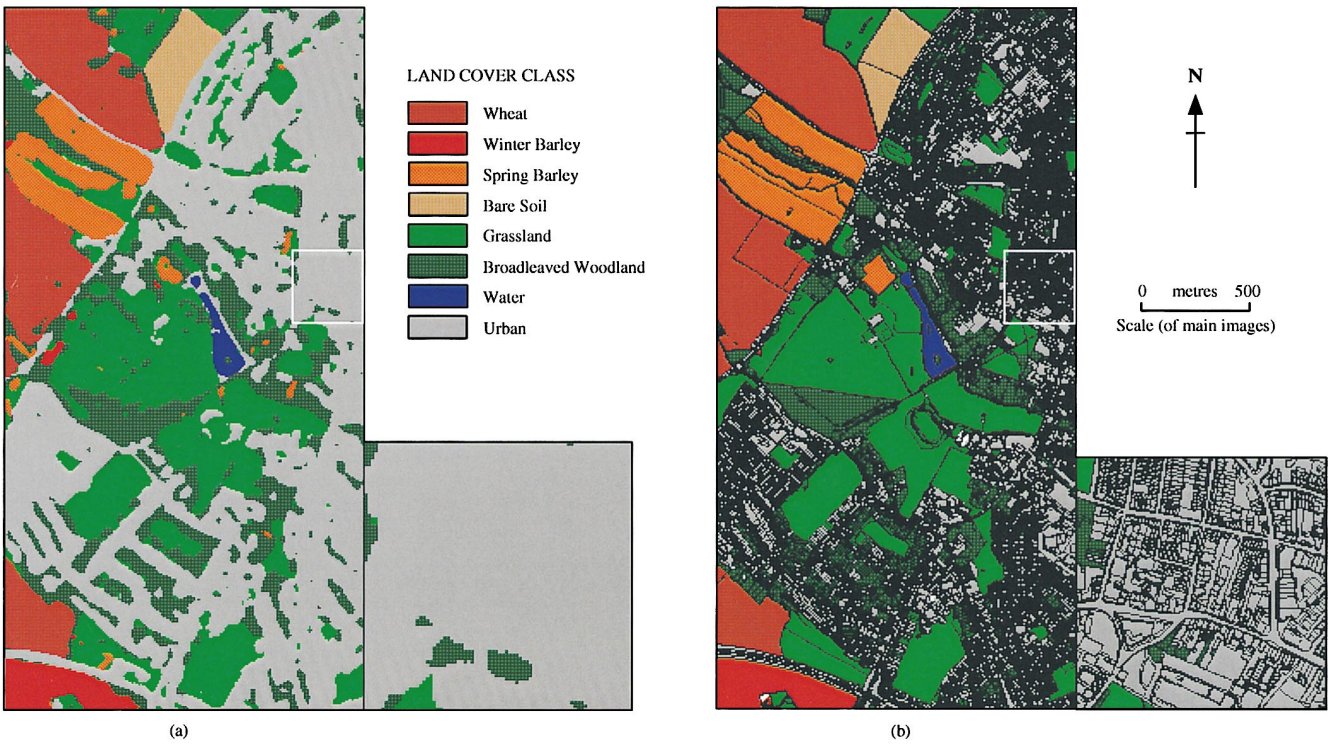

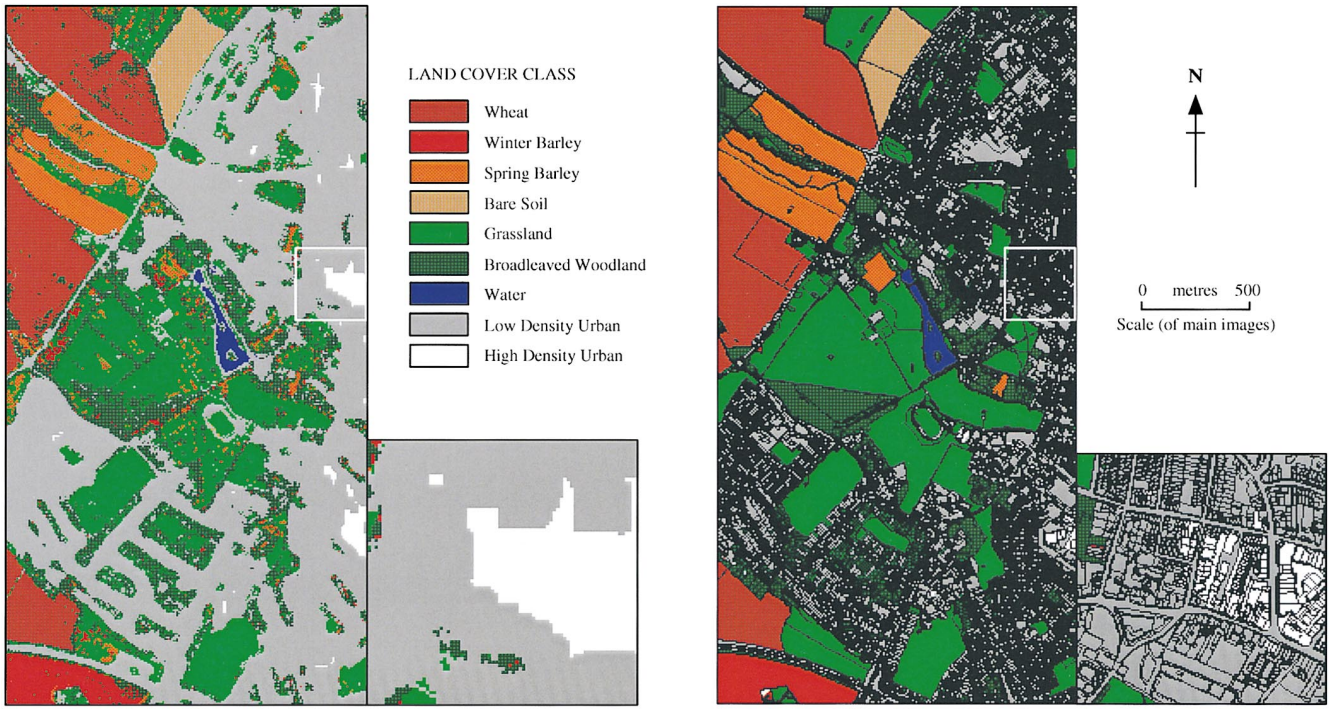

Figure 4. a) Per-pixel and b) per-field "texture" filtered classification of the study area. The black features in the per-field classificationare vector boundaries. To the bottom right of each of the main images is an enlargement of the urban area marked by the white box. (© Crown copyright. MC 1275. Used with permission.)

pixels of both broadleaved and conifer woodland occupied more than a specified proportion of a field a third class, mixed woodland, was assigned to the field (Aplin and Atkinson, 1997).

Second, an error flag was developed. Potential sources of classification error were highlighted by examining the proportion of each field occupied by the modal land cover. Where this proportion was relatively small (for example, less than 40%) misclassification was likely and manual checking could be performed. Figure 5 illustrates the proportion of each field of the per-field original classified image occupied by the modal land cover.

A fifth tool was proposed to indicate where field boundaries were missing or unclosed by comparing the local variance against the proportion of the modal land cover for each individual field. Where both the local variance and the proportion occupied by the modal land cover are small, there may be multiple homogenous patches of various land cover types (fields on the ground) and, therefore, missing boundaries.

Results

To assess classification accuracy, the reference land cover map was compared to each of the six classified images: the per-pixel original classification (Fig. 2a), the per-pixel smoothed classification (Fig. 3a), the per-pixel "texture" filtered classification (Fig. 4a), the per-field original clas-

Figure 5. Error flag: proportion of modal land cover class per field. The black features are vector boundaries. To the bottom right of the main image is an enlargement of the urban area marked by the white box. (© Crown copyright. MC 1275. Used with permission.)

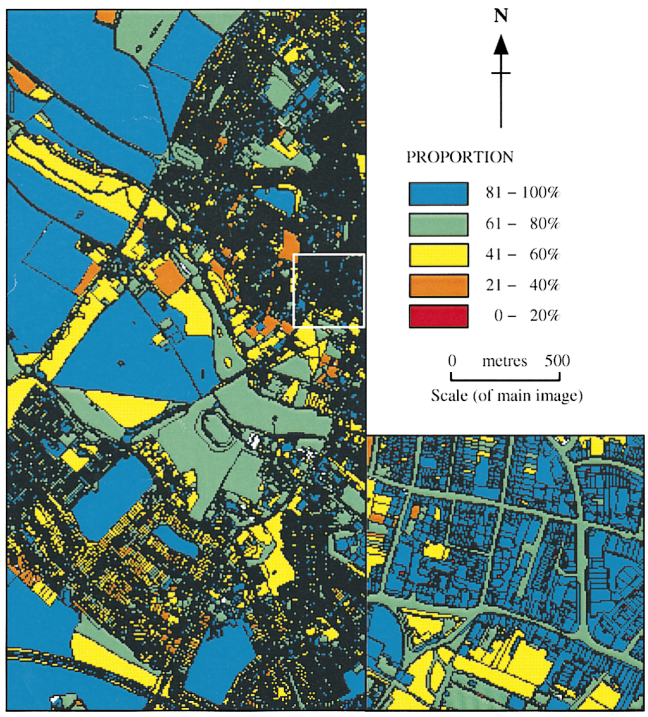

Table 2. Overall Classification Accuracies for Each of the Six Classifications

	Original P.P.[a]	*Smoothed P.P.*[a]	*"Texture" Filtered P.P.*[a]	*Original P.F.*[a]	*Smoothed P.F.*[a]	*"Texture" Filtered P.F.*[a]
Overall accuracy (%)	77.5	83.3	81.5	85.5	89	89.8

[a] P.P.=per-pixel classification and P.F.=per-field classification.

sification (Fig. 2b), the per-field smoothed classification (Fig. 3b), and the per-field "texture" filtered classification (Fig. 4b). For each classified image an equalized random sample of points was selected, whereby a constant number of points were selected randomly for each predicted class. This enabled a straightforward comparison of classification accuracy between classes. Each point was compared to the field to which it belonged on the reference land cover map to establish whether or not it had been classified correctly.

To illustrate the results, a series of tables presenting the overall classification accuracies (Table 2), the producer's and user's accuracies (Table 3), the confusion matrices (Tables 4a–4f) and the kappa coefficients (Table 5) of the six classifications are provided. Overall, per-field classification was more accurate than per-pixel classification for all three images. Also, per-pixel and per-field classification of the smoothed and "texture" filtered images were more accurate than their original counterparts.

In the original per-pixel and per-field classified image most of the misclassification occurred as a result of confusion between the urban class and grassland or broadleaved woodland. This illustrates the problem of classifying urban land cover from a mixture of various component land covers. By contrast the rural classes were generally classified with accuracies in excess of 90%.

Per-field classification resulted in a 7.5% increase in accuracy over per-pixel classification. The majority of this increase was due to the selection of the modal land cover in large rural fields at the per-field stage. This reduced spurious pixel-to-pixel misclassification (due to internal spectral variability within fields) that was present at the per-pixel stage. Further, the per-field classified images were more appealing visually and easier to interpret than the per-pixel classified images (Figs. 2b, 3b, and 4b compared to Figs. 2a, 3a, and 4a).

The per-pixel smoothed classification was more accurate than the per-pixel original classification for certain urban land covers (specifically, grassland and woodland), although the accuracy of the urban class itself remained constant. However, certain non-urban classes were classified less accurately. For instance, the accuracy for the water class decreased as a result of encroachment at the margins of water features by the smoothing process. One might wish to compare per-field classification to smoothing as a technique for reducing local spectral variability as in this case the per-field original classification was 2.2% more accurate than the per-pixel smoothed classification. Overall, however, the per-field smoothed classification was 3.5% more accurate than the per-field original classification.

The "texture" filtered classification was more accurate than the original and smoothed classifications for the urban class in both the per-pixel and per-field cases. Since non-urban areas were unaffected by the "texture" filter the accuracy of the rural classification was similar to the classification of the original image. Of the six classified images the per-field "texture" filtered classified image was the most accurate.

Slight misclassification occurred in all cases as a result of errors in geometric registration, the slight loss of geometric accuracy in rasterizing the Land-Line data and limitations in the sampling strategy employed. There is no evidence to suggest, however, that these limitations were not relatively constant between the six classified images.

Table 3. Producer's and User's Accuracies for Each Class, for Each of the Six Classifications[a]

	Original P.P.		*Smoothed P.P.*		*"Texture" Filtered P.P.*		*Original P.F.*		*Smoothed P.F.*		*"Texture" Filtered P.F.*	
Class	*Producer's Acc. (%)*	*User's Acc. (%)*	*Producer's Acc. (%)*	*User's Acc. (%)*	*Producer's Acc. (%)*	*User's Acc. (%)*	*Producer's Acc. (%)*	*User's Acc. (%)*	*Producer's Acc. (%)*	*User's Acc. (%)*	*Producer's Acc. (%)*	*User's Acc. (%)*
Wheat	94.2	98	94.3	100	90.7	98	96	96	100	96	100	98
Winter Barley	97	64	100	98	100	62	100	96	100	96	100	96
Spring Barley	100	64	97.5	78	91.1	82	100	94	100	98	98	98
Bare Soil	100	88	100	96	98	96	100	98	100	100	98	96
Grassland	59.7	80	69.5	82	62.3	76	76.5	78	84.9	90	84.9	90
Bl'd Wood.	61.5	32	84.6	22	65.6	42	77.8	28	95.5	42	88.9	48
Water	96.2	100	97.9	92	100	100	98	100	100	98	94.2	98
Urban	52.8	94	58.3	98	64	96	60.3	94	60.5	92	69.1	94

[a] P.P.=per-pixel classification and P.F.=per-field classification, Acc.=accuracy and Bl'd Wood.=broadleaved woodland.

Table 4a. Confusion Matrix of the Per-Pixel, Original Classification[a]

Predicted Class	*Reference Class*									
	Unclassified	*Wheat*	*Winter Barley*	*Spring Barley*	*Bare Soil*	*Grassland*	*Bl'd Wood.*	*Water*	*Urban*	*Total*
Unclassified	0	0	0	0	0	0	0	0	0	0
Wheat	1	49	0	0	0	0	0	0	0	50
Winter Barley	1	2	32	0	0	7	7	0	1	50
Spring Barley	1	0	1	32	0	14	1	0	1	50
Bare Soil	0	0	0	0	44	0	0	0	6	50
Grassland	0	0	0	0	0	40	1	0	9	50
Bl'd Wood.	2	1	0	0	0	6	16	0	25	50
Water	0	0	0	0	0	0	0	50	0	50
Urban	0	0	0	0	0	0	1	2	47	50
Total	5	52	33	32	44	67	26	52	89	400

[a] Bl'd Wood.=broadleaved woodland.

Table 4b. Confusion Matrix of the Per-Pixel, Smoothed Classification[a]

Predicted Class	*Reference Class*									
	Unclassified	*Wheat*	*Winter Barley*	*Spring Barley*	*Bare Soil*	*Grassland*	*Bl'd Wood.*	*Water*	*Urban*	*Total*
Unclassified	0	0	0	0	0	0	0	0	0	0
Wheat	0	50	0	0	0	0	0	0	0	50
Winter Barley	0	0	49	0	0	1	0	0	0	50
Spring Barley	1	0	0	39	0	9	0	1	0	50
Bare Soil	1	1	0	0	48	0	0	0	0	50
Grassland	1	0	0	1	0	41	1	0	6	50
Bl'd Wood.	3	2	0	0	0	7	11	0	27	50
Water	1	0	0	0	0	0	1	46	2	50
Urban	0	0	0	0	0	1	0	0	49	50
Total	7	53	49	40	48	59	13	47	84	400

[a] Bl'd Wood.=broadleaved woodland.

Table 4c. Confusion Matrix of the Per-Pixel, "Texture" Filtered Classification[a]

Predicted Class	*Reference Class*									
	Unclassified	*Wheat*	*Winter Barley*	*Spring Barley*	*Bare Soil*	*Grassland*	*Bl'd Wood.*	*Water*	*Urban*	*Total*
Unclassified	0	0	0	0	0	0	0	0	0	0
Wheat	0	49	0	0	0	0	0	0	0	50
Winter Barley	0	0	31	2	0	9	6	0	9	50
Spring Barley	0	0	0	41	0	8	1	0	8	50
Bare Soil	0	0	0	0	48	0	0	0	0	50
Grassland	1	0	0	1	1	38	2	0	0	50
Bl'd Wood.	2	5	0	1	0	6	21	0	6	50
Water	0	0	0	0	0	0	0	50	0	50
Urban	0	0	0	0	0	0	2	0	38	50
Total	3	54	31	45	49	61	32	50	61	400

[a] Bl'd Wood.=broadleaved woodland.

CONCLUSIONS

Within the next few years several fine spatial resolution satellite sensors will be launched. For example, QuickBird, IKONOS-1, and OrbView-3 will generate multispectral imagery with a spatial resolution of approximately 4 m. This article demonstrates the accuracy achievable in land cover classification using these sources of imagery. Six specific conclusions are drawn:

i. Per-field classification was more accurate than per-pixel classification, overcoming the problem of misclassification as a result of internal spectral variability within fields. Also, per-field classified

Table 4d. Confusion Matrix of the Per-Field, Original Classification[a]

	Reference Class									
Predicted Class	*Unclassified*	*Wheat*	*Winter Barley*	*Spring Barley*	*Bare Soil*	*Grassland*	*Bl'd Wood.*	*Water*	*Urban*	*Total*
Unclassified	0	0	0	0	0	0	0	0	0	0
Wheat	1	48	0	0	0	1	0	0	0	50
Winter Barley	1	0	48	0	0	0	0	0	1	50
Spring Barley	1	2	0	47	0	0	0	0	0	50
Bare Soil	0	0	0	0	49	0	1	0	0	50
Grassland	4	0	0	0	0	39	1	0	6	50
Bl'd Wood.	1	0	0	0	0	10	14	1	24	50
Water	0	0	0	0	0	0	0	50	0	50
Urban	0	0	0	0	0	1	2	0	47	50
Total	8	50	48	47	49	51	18	51	78	400

[a] Bl'd Wood.=broadleaved woodland.

Table 4e. Confusion Matrix of the Per-Field, Smoothed Classification[a]

	Reference Class									
Predicted Class	*Unclassified*	*Wheat*	*Winter Barley*	*Spring Barley*	*Bare Soil*	*Grassland*	*Bl'd Wood.*	*Water*	*Urban*	*Total*
Unclassified	0	0	0	0	0	0	0	0	0	0
Wheat	0	48	0	0	0	1	1	0	0	50
Winter Barley	2	0	48	0	0	0	0	0	1	50
Spring Barley	0	0	0	49	0	1	0	0	0	50
Bare Soil	0	0	0	0	50	0	0	0	0	50
Grassland	2	0	0	0	0	45	0	0	3	50
Bl'd Wood.	0	0	0	0	0	3	21	0	26	50
Water	0	0	0	0	0	0	0	49	1	50
Urban	1	0	0	0	0	3	0	0	46	50
Total	5	48	48	49	50	53	22	49	76	400

[a] Bl'd Wood.=broadleaved woodland.

Table 4f. Confusion Matrix of the Per-Field, "Texture" Filtered Classification[a]

	Reference Class									
Predicted Class	*Unclassified*	*Wheat*	*Winter Barley*	*Spring Barley*	*Bare Soil*	*Grassland*	*Bl'd Wood.*	*Water*	*Urban*	*Total*
Unclassified	0	0	0	0	0	0	0	0	0	0
Wheat	0	49	0	0	0	1	0	0	0	50
Winter Barley	1	0	48	1	0	0	0	0	0	50
Spring Barley	0	0	0	49	0	1	0	0	0	50
Bare Soil	0	0	0	0	48	0	0	1	0	50
Grassland	0	0	0	0	0	45	1	0	4	50
Bl'd Wood.	1	0	0	0	0	6	24	2	17	50
Water	0	0	0	0	1	0	0	49	0	50
Urban	1	0	0	0	0	0	2	0	47	50
Total	3	49	48	50	49	53	27	52	68	400

[a] Bl'd Wood.=broadleaved woodland.

images were easier to interpret visually than per-pixel classified images.

ii. A low pass smoothing filter increased the accuracy of classifying urban land cover but decreased the accuracy of classifying some non-urban land cover.

iii. A "texture" filter increased the accuracy of classifying urban land cover without affecting non-urban land cover and enabled the production of new land cover classes based on the amount of local texture present.

iv. The flexibility of the integration process enabled

Table 5. Kappa Coefficients for Each of the Six Classifications

Class	*Original P.P. Kappa Coefficients*	*Smoothed P.P. Kappa Coefficients*	*'Texture' Filtered P.P. Kappa Coefficients*	*Original P.F. Kappa Coefficients*	*Smoothed P.F. Kappa Coefficients*	*'Texture' Filtered P.F. Kappa Coefficients*
Unclassified	0.0000	0.0000	0.0000	0.0000	0.0000	0.0000
Winter Wheat	0.9770	1.0000	0.9769	0.9543	0.9545	0.9772
Winter Barley	0.6076	0.9772	0.5881	0.9545	0.9545	0.9545
Spring Barley	0.6087	0.7556	0.7972	0.9320	0.9772	0.9771
Bare soil	0.8652	0.9545	0.9544	0.9772	1.0000	0.9544
Grass	0.7598	0.7889	0.7168	0.7479	0.8847	0.8847
Bl'd Wood.	0.2727	0.1938	0.3696	0.2461	0.3862	0.4424
Water	1.0000	0.9093	1.0000	1.0000	0.9772	0.9770
Urban	0.9228	0.9747	0.9508	0.9255	0.9012	0.9277
Overall Kappa Coefficients	0.7433	0.8090	0.7888	0.8348	0.8745	0.8830

[a] P.P.=per-pixel classification and P.F.=per-field classification, and Bl'd Wood.=broadleaved woodland.

the exploitation of spectral and spatial variation between pixels within individual fields and new useful classes (such as mixed woodland) were produced at the per-field stage.

v. The proportion of each field occupied by the modal land cover was used as an "error flag" to identify fields with a high likelihood of misclassification.

vi. Missing or unclosed field boundaries could be identified by comparing local variance to the proportion of modal land cover within individual fields.

This work was undertaken as part of a British National Space Centre and Ordnance Survey funded Applications Demonstration Programme entitled Landuse and National Digital Mapping from Advanced Satellite Sensors (LANDMASS). The authors thank Atlantic Reconnaissance for acquiring the CASI imagery, the Natural Environment Research Council (NERC) Equipment Pool for Field Spectroscopy (EPFS) for supplying the spectroradiometer, the residents and land owners at the field site who provided land cover information, the team of fieldworkers who mapped the land cover of the field site, and the GeoData Institute, University of Southampton, and Jim Milne for assistance with computing. A preliminary version of this article was presented for discussion at the seventh International Symposium of the International Society for Photogrammetry and Remote Sensing (ISPRS) on Physical Measurements and Signatures in Remote Sensing in Courchevel, France on 10 April 1997 (Aplin et al., 1997b).

REFERENCES

Aplin, P., and Atkinson, P. M. (1997), *Work Package 6 Completion Report, Application Demonstration Program—Landuse And National Digital Mapping from Advanced Satellite Sensors (LANDMASS)* Ordnance Survey, Southampton.

Aplin, P., Atkinson, P. M., and Curran, P. J. (1997a), Fine spatial resolution satellite sensors for the next decade. *Int. J. Remote Sens.* 18:3873–3881.

Aplin, P., Atkinson, P. M., and Curran, P. J. (1997b), Using the spectral properties of fine spatial resolution satellite sensor imagery for national land cover and land use mapping. In *Physical Measurements and Signatures in Remote Sensing* (E. Guyot and T. Phulpin, Eds.), Balkema, Rotterdam, pp. 661–668.

Babey, S. K., and Soffer, R. J. (1992), Radiometric calibration of the Compact Airborne Spectrographic Imager (CASI). *Can. J. Remote Sens.* 18:233–242.

Catlow, D. R., Parsell, R. J., and Wyatt, B. K. (1984), The integrated use of digital cartographic data and remotely sensed imagery. *Earth-Orientated Appl. Space Technol.* 4:255–260.

Congalton, R. G. (1997), Exploring and evaluating the consequences of vector-to raster and raster-to-vector conversion. *Photogramm. Eng. Remote Sens.* 63:425–434.

Cowen, D. J., Jensen, J. R., Bresnahan, P. J. (1995), The design and implementation of an integrated geographic information system for environmental applications. *Photogramm. Eng. Remote Sens.* 61:1393–1404.

Curran, P. J. (1994), Imaging spectrometry. *Prog. Phys. Geogr.* 18:247–266.

Cushnie, J. L. (1987), The interactive effect of spatial resolution and degree of internal variability within land-cover types on classification accuracies. *Int. J. Remote Sens.* 8:15–29.

Davis, F. W., Quattrochi, D. A., Ridd, M. K., et al. (1991), Environmental analysis using integrated GIS and remotely sensed data: some research needs and priorities. *Photogramm. Eng. Remote Sens.* 57:689–697.

Ehlers, M., Greenlee, D., Smith, T., and Star, J. (1991), Integration of remote sensing and GIS: data and data access. *Photogramm. Eng. Remote Sens.* 57:669–675.

ESRI (1993), *ARC Command References J-Z*, Environmental Systems Research Institute, Redlands.

Fuller, R. M., Sheail, J., and Barr, C. J. (1994), The land of Britain, 1930–1990: a comparative study of field mapping and remote sensing techniques. *Geogr. J.* 160:173–184.

Harris, P. M., and Ventura, S. J. (1995), The integration of geographic data with remotely sensed imagery to improve classification in an urban area. *Photogramm. Eng. Remote Sens.* 61:993–998.

Hinton, J. C. (1996), GIS and remote sensing for environmen-

tal applications. *Int. J. Geographical Information Systems.* 10:877–890.

Janssen, L. L. F., and Molenaar, M. (1995), Terrain objects, their dynamics and their monitoring by the integration of GIS and remote sensing. *IEEE Trans. Geosci. Remote Sens.* 33:749–758.

Janssen, L. L. F., Jaarsma, M. N., and Van der Linden, T. M. (1990), Integrating topographic data with remote sensing for land-cover classification. *Photogramm. Eng. Remote Sens.* 56:1503–1506.

Johnsson, K. (1994), Segment-based land-use classification from SPOT satellite data. *Photogramm. Eng. Remote Sens.* 60:47–53.

Lobo, A., Chic, O., and Casterad, A. (1996), Classification of Mediterranean crops with multisensor data: per pixel versus per-object statistics and image segmentation. *Int. J. Remote Sens.* 17:2385–2400.

Mason, D. C., Corr, D. G., Cross, A., et al. (1988), The use of digital map data in the segmentation and classification of remotely-sensed images. *Int. J. Remote Sens.* 2:195–215.

Mégier, J., Mehl, W., and Rupelt, R. (1984), Per-field classification and application to SPOT simulated, SAR and combined SAR-MSS data. In *Proceedings of the 18th International Symposium on Remote Sensing of Environment*, University of Michigan, Ann Arbor, pp. 1011–1018.

Ortiz, M. J., Formaggio, A. R., and Epiphanio, J. C. N. (1997), Classification of croplands through integration of remote sensing, GIS, and historical database. *Int. J. Remote Sens.* 18:95–105.

Pedley, M. I., and Curran, P. J. (1991), Per-field classification: an example using SPOT HRV imagery. *Int. J. Remote Sens.* 12:2181–2192.

Ryherd, S., and Woodcock, C. (1996), Combining spectral and texture data in the segmentation of remotely sensed images. *Photogramm. Eng. Remote Sens.* 62:181–194.

Townshend, J. R. G. (1981), The spatial resolving power of Earth resources satellites. *Prog. Phys. Geogr.* 5:32–55.

Townshend, J. R. G. (1992), Land cover. *Int. J. Remote Sens.* 13:1319–1328.

White, J. D., Kroh, G. C., and Pinder, J. E., III (1995), Forest mapping at Lassen Volcanic National Park, California, using Landsat TM data and a geographical information system. *Photogramm. Eng. Remote Sens.* 61:299–305.

Wilkinson, G. G. (1996), A review of current issues in the integration of GIS and remote sensing data, *Int. J. Remote Sens.* 10:85–101.